forests

MDPI

Article

A GIS-Based Decision Support Model (DSM) for Harvesting System Selection on Steep Terrain: Integrating Operational and Silvicultural Criteria

Benno Eberhard [1,*], Zoran Trailovic [2], Natascia Magagnotti [1] and Raffaele Spinelli [1]

[1] Italian National Research Council-Institute of BioEconomy (CNR IBE), 50019 Sesto Fiorentino, Italy; natascia.magagnotti@ibe.cnr.it (N.M.); raffaele.spinelli@ibe.cnr.it (R.S.)
[2] Austrian Federal Forests (ÖBf), 3002 Purkersdorf, Austria; trailovich@gmail.com
* Correspondence: benno.eberhard@ibe.cnr.it

Abstract: The goal of this study was to develop a GIS-based Decision Support Model for selecting the best timber harvesting systems on steep terrain. The model combines multiple layers, each representing an important factor in mechanized logging. These layers are used to create a final map that functions as a spatially explicit Decision Support Model that helps decide which machines are best suited for different forest areas. A key idea of this study is to consider not only operational criteria (slope, ruggedness, wetness, and road accessibility), but also a fundamental silvicultural aspect, i.e., the assessment of tree growth classes to enable the integration of silvicultural deliberations into timber harvest planning. The data used for this model come from orthophoto image and a Digital Terrain Model (DTM). The operational factors were analyzed using GIS tools, while the silvicultural aspects were assessed using the deep learning algorithm DeepForest and tree growth equations (allometric functions). The model was tested by comparing its results with field data taken in a Norway Spruce stand in South Tyrol/Italy. The findings show that the model reliably evaluates operational factors. For silvicultural aspects, it tends to underestimate the number of small trees, but provides a good representation of tree size classes within a forest stand. The innovation of this method is that it relies on low-cost, open-source tools instead of expensive 3D scanning devices.

Keywords: remote sensing in forestry; decision support system; GIS-based forest; management; orthophoto image; R-CNN-based tree detection; operational criteria for mechanized harvesting; allometric equation for tree diameter; silvicultural planning

Academic Editor: Chong Xu

Received: 2 April 2025
Revised: 9 May 2025
Accepted: 16 May 2025
Published: 20 May 2025

Citation: Eberhard, B.; Trailovic, Z.; Magagnotti, N.; Spinelli, R. A GIS-Based Decision Support Model (DSM) for Harvesting System Selection on Steep Terrain: Integrating Operational and Silvicultural Criteria. *Forests* **2025**, *16*, 854. https://doi.org/10.3390/f16050854

1. Introduction

Logging operations on steep terrain present significantly greater challenges compared to those conducted on gentle slopes, due to increased risks of environmental damage, higher operational costs, greater technical complexities, and more severe worker safety issues [1,2]. As a result, it becomes critical to carefully select the most appropriate harvesting system for such conditions. In that regard, operators face two main alternatives: ground-based machine systems and cable-based machine systems.

Ground-based machine systems (GBSs) are generally associated with higher productivity levels, due to their efficiency in accessing and processing timber [3]. Cable-based machine systems (CBSs) result in significantly less stand damage, which makes them preferable in ecologically sensitive areas [4,5]. However, cable-based machinery is the more cost-intensive variant [6,7]. The challenge lies in identifying the optimal system

for each particular site, one that achieves a balance between high productivity and low environmental impact.

That decision can be guided by five key operational criteria: slope gradient, soil bearing capacity, geomorphological hindrances (the ground obstacles, such as rocks or debris), the existing forest road network, and sensitive zones that are restricted from timber harvesting, including stream management zones (SMZs), biotopes, and other special protection areas [8]. Those criteria collectively influence the feasibility, safety, and environmental impact of the chosen harvesting system [9].

In a best-practice approach, these five factors would be brought together to improve harvesting planning. Furthermore, such an approach would include another important aspect for successful forest operations—the basic silvicultural characteristics of the stand, with a focus on how tree diameters are distributed across different areas of the forest. While previous studies [10,11] have examined this factor mainly for selecting appropriate machinery—since each type has limits in handling certain tree sizes—this study takes a different approach. Here, the goal is to integrate silvicultural considerations into operational planning, helping forest managers align harvesting decisions with more holistic forest management objectives.

An effective way to bring these factors together is by using remote sensing. This approach evaluates the six key factors for each pixel of the forest area using geospatial data. It is designed to support decision making while explicitly requiring the forest manager's judgment—especially in setting thresholds that define acceptable harvesting conditions. For instance, even if a steep slope permits mechanized operations, they must also be environmentally appropriate. To reduce soil damage, a slope limit can be defined for ground-based machines. If that limit is exceeded, a cable-based system should be preferred.

Several previous studies have explored key aspects of the here-presented approach. Some of them were dedicated to individual tree detection based on remotely sensed data, integrating different methods for data acquisition and processing. Several studies have relied on unmanned aerial vehicle (UAV)-based imagery, e.g., Gan et al. [12] used UAV red–green–blue (RGB) imagery to detect trees in a temperate deciduous forest, using the DeepForest neural network and the Detectree2 neural network. Fu et al. [13] employed UAV imagery to detect tree crowns and tree heights using a Mask Region-based Convolutional Neural Network (Mask R-CNN) deep learning-based instance segmentation model. Allometric functions were applied to predict tree diameter (Diameter at Breast Height, DBH) and tree biomass based on detected tree height and tree crown dimensions. An improved Mask R-CNN deep learning model, based on UAV imagery for tree detection and species classification in mixed forests, was also applied by Zhang et al. [14]. Sivanandam et al. [15] captured data using a combination of UAV RGB and multispectral imagery in a mixed-species forest, applying neural networks (Convolutional Neural Networks, CNNs) for tree detection. Persson [16] also used drone-acquired imagery for tree crown detection, applying the DeepForest neural network. Other studies have used Light Detection and Ranging (LiDAR)-based data, e.g., Wang et al. [17] captured LiDAR data from a complex forest ecosystem and processed it using CNN-based deep learning for tree detection. Other studies have combined UAV-based RGB imagery and LiDAR data. Bennett et al. [18] applied this method in wildfire-prone forests, using the DeepForest algorithm for tree detection and classification. Another approach involves satellite- or plane-based imagery as a basis for the detection of individual trees. Freudenberg et al. [19] used Sentinel-2 imagery and applied machine learning classifiers for tree detection and tree species classification across Germany. Beloiu et al. [20] captured orthophotos from aerial imagery and applied CNN-based deep learning for tree detection, using a customized deep learning model.

Another group of studies developed mapping procedures as decision supports for the selection of a suitable harvesting system. Klosterhuber et al. [21] analyzed harvesting systems in South Tyrol, focusing on road networks, slope gradients, geomorphology, and cost-efficiency as operational criteria. They took ecological aspects into consideration, but did not integrate forest stand criteria that would enable silvicultural planning. Phelps et al. [22] developed a GIS-based tool for wheel-based harvesting machinery, considering slope, skidding distance, and the stand age as a proxy for timber volume. This procedure does not allow for fine-scale silvicultural recommendations. Bont et al. [6] created a decision tool incorporating GIS, National Forest Inventory (NFI) data, and decision trees to optimize harvesting system selection, but excluded forest stand analysis based on individual tree detection.

Collectively, these studies call for the integration of the described operational and silvicultural factors into a streamlined procedure. Such a framework would utilize (i) orthophotos with three spectral bands for tree detection, instead of drone-captured images; (ii) the open-source DeepForest Python module (version 1.3.3) for tree crown identification; (iii) allometric functions to estimate tree diameters based on crown dimensions; (iv) a Digital Terrain Model (DTM) and a Digital Surface Model (DSM-surface) for site assessments; and (v) open-source GIS software for mapping criteria.

In doing so, the novelty of the proposed method lies in its budget-friendly approach, requiring only three initial raster layers, an orthophoto image, a DTM and a DSM-surface, and the use of an open-source computer vision algorithm, combined with a silvicultural focus to guide the selection of the harvesting system and the operational and silvicultural planning.

The following two main assumptions shaped this study: (i) a focus on highly mechanized logging systems; and (ii) the exclusion of cost, productivity, and efficiency analyses, as the present study aimed to assess technical feasibility rather than economic aspects.

2. Materials and Methods

2.1. Generating the GIS-Based Decision Support Model

For the scope of this study, the model should display the operability and a baseline silvicultural feature for each point of a forest area. Based on these characteristics, the model should provide guidance on the appropriate machinery type for ensuring a successful harvesting operation.

Before detailing the setup of the Decision Support Model, the following flowchart (Figure 1) provides a structured overview of the work steps undertaken for the development, implementation, and evaluation of the model.

The geospatial tool was built using GIS technology, incorporating two platforms: QGIS (version 3.38.2) [23], which integrates tools from SAGA GIS (version 9.5.1) [24], and GRASS GIS (version 8.4.0) [25]. Since six criteria were considered, five related to site characteristics—the operational criteria—and one to stand conditions—the silvicultural criterion—the final model was composed of six layers. To execute the model, these layers were overlaid by applying spatial decision rules implemented within the GRASS GIS environment. Each of the six criteria was assigned equal weight, ensuring that no single data layer had greater influence over the others.

The following machinery was considered as being representative for the two major categories of timber extraction on steep terrain: (1a) a standard harvester–forwarder system (wheeled or tracked), in which felling and processing are conducted by the harvester and extraction by the forwarder [5,26]; (1b) a winch-assisted harvester–forwarder system, in which the machines are tethered by a winch for use in steep terrain [27]; and (2) a tower yarder system, in which felling is performed motor-manually with chainsaws, extraction

by a tower yarder, and processing by a roadside processor (possibly integrated within the tower yarder unit) [5,26].

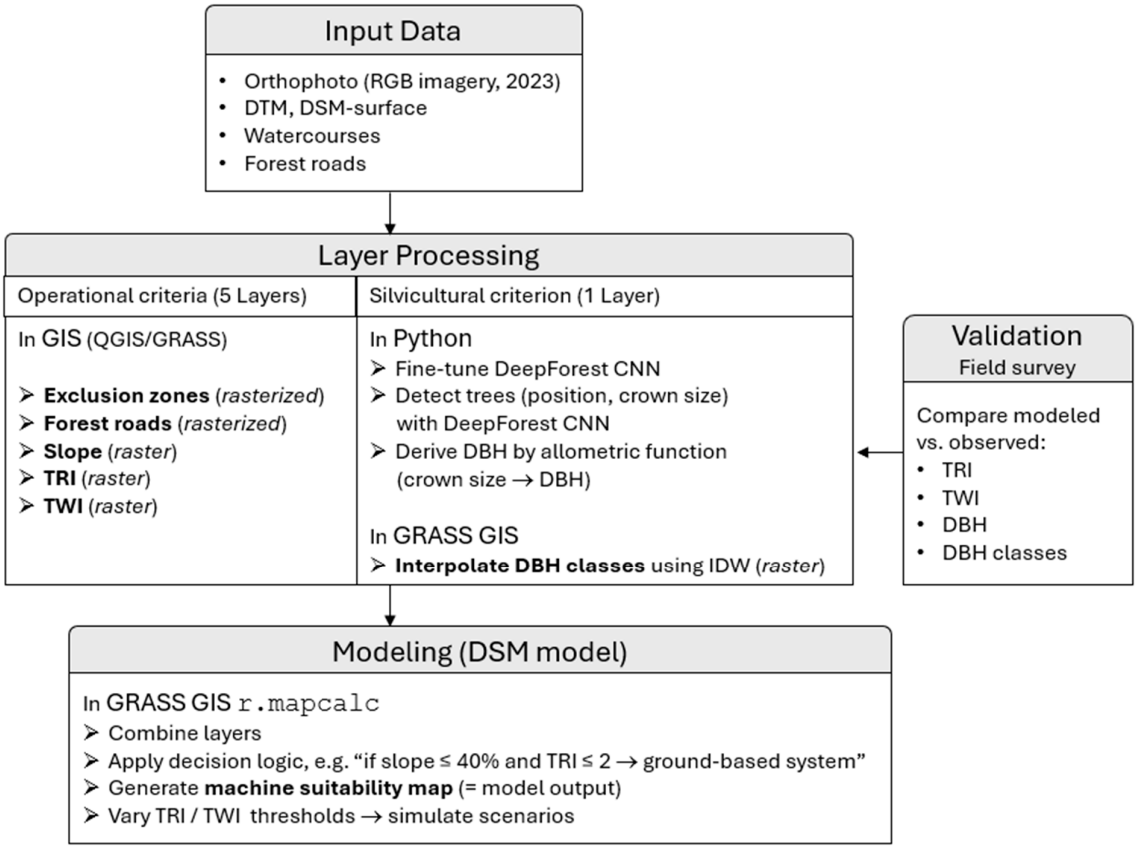

Figure 1. Workflow for developing the GIS-based Decision Support Model (DSM) for harvesting system selection based on operational and silvicultural criteria. DTM stands for Digital Terrain Model, DSM-surface refers to the Digital Surface Model, DSM (in our study) denotes the Decision Support Model, TRI is the Terrain Ruggedness Index, TWI is the Topographic Wetness Index, DBH is Diameter at Breast Height, CNN stands for Convolutional Neural Network, and IDW is Inverse Distance Weighting.

2.2. Generation of the Six Layers for the Model

The following raster layers were generated for each of the six criteria to allow spatially explicit predictions for every point within a given area:

(i) The first layer delineated the network of watercourses within the study area, based on available cartographic data.

(ii) The second layer represented the forest road net. To address soil protection concerns, areas for ground-based logging were limited to a certain distance from forest roads. Areas beyond this distance were categorized as suitable for cable-based systems. This range was delineated using the GRASS GIS tool `r.grow.distance`.

(iii) The third layer, representing slope, was calculated based on a Digital Terrain Model (DTM) at a spatial resolution of 2.5 m × 2.5 m.

(iv) The fourth layer captured terrain ruggedness, a critical factor for ground-based extraction systems, calculated using the topographic ruggedness index (TRI) [28] within the SAGA GIS environment. The TRI measures the variability in elevation around a specific pixel by calculating the standard deviation of elevations of the neighboring pixels. Parameters were adjusted to reduce sensitivity to abrupt elevation changes, using a linear weighting function for the impact of the distance of pixels around a

reference pixel, and a 12.5 m × 12.5 m calculation window was used to ensure a generalized terrain assessment.

(v) The fifth layer assessed soil-bearing capacity. Since no detailed information on the soil type of the chosen study area was available, the Topographic Wetness Index (TWI), developed by Beven et al. [29], was used as a proxy for factors like precipitation, permeability, vegetation, and soil type. Specifically, it estimates the potential for soil moisture accumulation in the landscape and is calculated according to the following equation:

$$\mathrm{TWI} = \ln\left(\frac{A_S}{\tan(\beta)}\right) \quad (1)$$

where A_s is the upslope contributing area (m^2/m), and β is the slope angle (radians).

(vi) The sixth layer was on the distribution of Diameter at Breast Height (DBH) classes. This layer is essential for enabling silvicultural examinations. The process consisted of the following three main steps:

Step 1: Setting up the DeepForest algorithm and tree crown detection once the algorithm was ready

Tree detection was performed using DeepForest, an open-source deep learning algorithm based on Region-Based Convolutional Neural Networks (R-CNNs) [30]. It detects tree crowns from aerial imagery such as orthophotos and allows for fine-tuning with custom datasets. The algorithm was applied in the following way: A test section of the study area was selected, and predictions were made using the built-in model. Ground truth of that section was created using the open-source Python package LabelMe [31]. Finally, based on the ground truth, the model was fine-tuned by setting the following hyperparameters: 10 epochs, a learning rate of 0.001, and a batch size of 4. The output was validated using the F1 score [32]. Before running the fine-tuned algorithm, the orthophoto was divided into sub-tiles to maintain accuracy. The tree positions were identified as crown centers, and the crown diameters were calculated as the average of the rectangle sides. The data were then reprojected to EPSG:25832 (ETRS89, UTM Zone 32N) for GIS integration.

Step 2: DBH calculation by allometric functions

The DBH of detected trees was estimated based on the crown dimensions. Three allometric equations were tested, and the following one, which demonstrated the best validation performance, was selected for further use:

$$DBH = e^{\frac{\ln(CW)-(-0.3232)}{0.6441}} \quad (2)$$

$$DBH = 0.557 \times (h \times CW)^{0.809} \times e^{\frac{0.056^2}{2}} \quad (3)$$

$$DBH = e^{\frac{\log(CA)-(-1.43)}{1.2}} \quad (4)$$

where CW = crown width (m), h = tree height (m), and CA = crown area (m^2). Equation (1) presents the model by Hasenauer [33], Equation (2) refers to that of Jucker et al. [34], and Equation (3) to that of Pretzsch et al. [35].

The tree heights needed for Equation (3) were calculated using a Canopy Height Model (CHM), which was generated by subtracting the Digital Terrain Model (DTM) from the Digital Surface Model (DSM-surface).

Step 3: Mapping the DBH classes

Once the DBH values were obtained, they were transformed into spatial data using the Inverse Distance Weighting (IDW) interpolation method in GRASS GIS, which created a continuous DBH surface. Diameter values were classified into the following three groups: 11–20 cm: Pole-stage wood; 21–50 cm: Tree wood; and >50 cm: Old growth [36,37].

2.3. Model Implementation

To run the model, predefined thresholds for harvesting systems were set based on terrain limits and operational constraints. A buffer of 10 m on either side of all watercourses was excluded from harvesting activities to protect riparian vegetation and minimize soil disturbance [38]. Since soil disturbance and compaction are essentially influenced by the number of passes of the machines [39,40] we decided for a rather conservative approach and deemed that only areas within 200 m of roads suitable for ground-based systems. Standard harvester–forwarder systems were suitable for slopes up to 40%, while winch-assisted systems could operate on slopes up to 100%. For slopes above 100%, only cable-based systems were viable. Above 150%, no operations can be executed [41–43]. Low-impact ground-based operations required TRI $\leq$ 1 and TWI $\leq$ 5 to minimize environmental damage. If a higher impact was acceptable, the TRI could go up to 2 and the TWI up to 10 [44]. Ground-based and cable-based systems encompassed two distinct size classes: a small-scale application, designed to efficiently handle logs with a mean diameter of up to 20 cm, and a large-scale application, tailored for processing logs with diameters exceeding 20 cm. Since thinning is a key part of the silvicultural treatment of a stand, and usually happens when trees reach a certain minimum size, we excluded trees with a diameter smaller than 10 cm from the analysis [45].

The listed thresholds were implemented into the model using the GRASS GIS tool `r.mapcalc`. This algorithm allows pixel-wise raster calculation via nested if() statements that evaluate each pixel according to predefined threshold settings (slope, TRI, TWI, DBH class, and proximity to roads and water). A simplified example of this logic is:

if slope $\leq$ 40 AND TRI $\leq$ 2 AND TWI $\leq$ 10 $\rightarrow$ Use standard harvester

else if slope $\leq$ 100 $\rightarrow$ Use winch-assisted harvester

else $\rightarrow$ Use cable system

For details on GRASS GIS syntax and methods, refer to the official documentation [25] and tutorials [46].

2.4. Model Validation

The model was applied to a test area, and its predictions were verified through on-site field measurements. To select the observation plots in the field, a systematic grid was generated using standard vector editing and geoprocessing functions in QGIS to establish 30 fixed observation plots across the study area. Each plot had a diameter of 15.96 m, covering an area of 200 m^2. The following parameters were recorded: tree species, Diameter at Breast Height (DBH) of each tree, and the height of the tree with the median diameter. Furthermore, within these plots, two model outcomes were verified: the operational predictions and the silvicultural forecasts.

To test the operational predictions, two key parameters were evaluated: the Topographic Wetness Index (TWI), depicting the ground-bearing capacity; and the Terrain Ruggedness Index (TRI), symbolizing obstacles. At the selected observation plots, experts determined whether each location was harvestable or not harvestable. If the field assessment confirmed the area was operable, and the model predicted a TWI value of 10 or below, it was considered a match; if the model value exceeded 10, it was a mismatch. Similarly,

if experts confirmed that the terrain was passable for ground-based machinery and the model predicted a value of 2 or below, it was a match; otherwise, it was a mismatch.

For the validation of the silvicultural predictions of the model, it was of utmost interest to select the most accurate of the three equations applied for deriving the tree diameter based on crown size. To compare the outputs of each of the three equations with the values sampled on the ground, the two-sample Anderson–Darling test [47] was employed, as it is sensitive to differences in the tails of data distributions, making it particularly useful when checking whether deviations are increasing at lower or higher values. Moreover, Pearson's correlation coefficient was calculated to test for linear relationships between the predicted and the observed diameter values. In addition, the following error metrics were adopted: the mean absolute error (MAE), the mean bias error (MBE), and the normalized root mean square error (NRMSE) [48]. Each equation underwent this testing, and the one providing the closest alignment to the empirical data was adopted. Since it is known from other studies that the accuracy of models like the one developed in this context (i.e., including a CNN deep learning algorithm that detects trees based on orthophotos) tends to decrease at smaller dimensions of trees [16,20], an additional objective was to evaluate whether the algorithm disproportionately overlooked small trees compared to more advanced growth classes. For that purpose, the frequencies of the single DBH classes (10–20 cm, 21–50 cm, >50 cm), according to the three equations, were calculated and compared with the observed values. Finally, to evaluate the model's spatial predictions on DBH classes across the test area, the model output was compared with the 50th percentile of the diameters within a test plot. To give an example, if the model predicted a diameter class of 21–50 cm for a given patch, and the observed median diameter was within this range (e.g., 35 cm), it was classified a match.

2.5. Data

All layers for model generation (Table 1) were retrieved from a regional cartographic resource, the South Tyrolean Citizen Network (Mapview Portal) [49]. All raster datasets were provided as GeoTIFF files with a spatial resolution of 2.5 m × 2.5 m. The orthophoto image contained three spectral bands (red, green, blue). Vector datasets (watercourses and road networks) were provided in the ESRI Shapefile format, with polyline topology.

Table 1. Overview of the input data layers used for model generation.

Name of Layer	Type of Layer	Format	Resolution/Bands
Orthophoto image Aerial-2023-RGB	Raster	GeoTIFF	2.5 m × 2.5 m 3 bands (RGB)
Digital Terrain Model South Tyrol	Raster	GeoTIFF	2.5 m × 2.5 m 1 band (elevation)
Digital Surface Model South Tyrol	Raster	GeoTIFF	2.5 m × 2.5 m 1 band (surface h)
Watercourses	Vector (Line)	ESRI Shape	Typology: Polyline
Road net	Vector (Line)	ESRI Shape	Typology: Polyline

2.6. Test Area

The 91.2-hectare test area is located in the municipality of Rasen-Antholz/Rasun-Anterselva, in South Tyrol, Italy. The center of the area has the coordinates 46°46′44″ N, 12°3′57″ E (EPSG:4326—WGS 84). It has an alpine climate, with cold, snowy winters (over the years since registration, the average minimum temperature in the coldest month is −9 °C) and mild summers (over the years since registration, the average maximum temperature in the warmest month is 25 °C). The area receives an average annual precipitation of 986 mm, according to the Office for Meteorology and Avalanche Warning, Autonomous Province of Bolzano [50]. The terrain consists of a steep, north-facing slope ranging from 1108 m to 1495 m above sea level, with an average incline of 48%. The forest is predom-

inantly composed of Norway spruce (*Picea abies* (L.) H. Karst.), with silver fir (*Abies alba* Mill.) and European larch (*Laric decidua* Mill.) as admixed species. Two key characteristics define this forest. First, its fragmented ownership structure results in inconsistent forest management across different parcels. Second, increasing bark beetle infestations in recent years have led to widespread salvage logging through clear-cutting in affected areas. These factors have contributed to a highly uneven-aged forest structure, shaped by small-scale management interventions and natural disturbance-driven regeneration. This woodlot was suitable for the present study because it features both steep slopes and gentle sections, along with waterways and a network of forest roads, altogether matching the criteria meant to be integrated into the model. Figure 2 shows the study site and the established plots for the field observations:

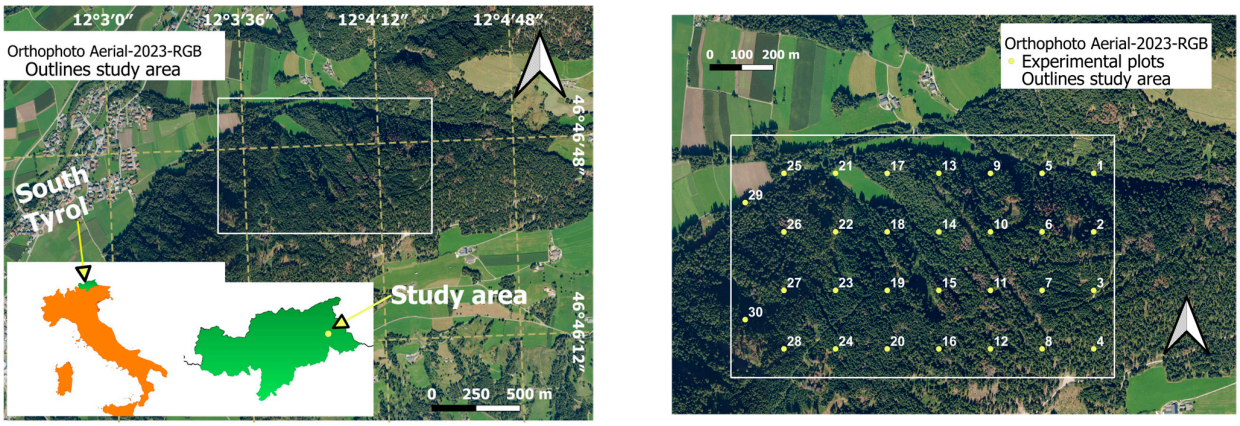

Figure 2. Overview of the study area in Rasen-Antholz, South Tyrol, Italy. White points denote the 30 experimental plots for field survey. Inset shows the location of the study area within South Tyrol. Basemap source: South Tyrolean Citizen Network (Mapview Portal) [49]; orthophoto acquired in 2023.

In addition to GIS-based methods, the Python programming language [51] was used for the analyses. The DeepForest algorithm (Python module) and the annotation tool LabelMe were employed for tree crown detection and manual image labeling, respectively. Data processing, visualization, and evaluation were carried out with the support of open-source Python libraries, including `numpy`, `scipy`, `pandas`, `matplotlib`, and `scikit-learn`.

3. Results

3.1. Layers Determining the Operational Site Conditions

The forest roads and watercourses within the experimental site are shown in Figure 3A. For the illustration of the slope (Figure 3B), the values were grouped into the following three functional classes: up to 40%, 40%–100%, and >100%. The Topographic Ruggedness Index (TRI) is illustrated in Figure 3C. The TRI values range from 0.006 to 4.237. Figure 3D presents the Topographic Wetness Index (TWI). The TWI values range from 0.0 to 18.841.

Out of the 30 plots, 28 could be sampled, since one fell into agricultural land (plot 21, see Figure 2), and one was inaccessible due to the steepness of the terrain (plot 30, see Figure 2).

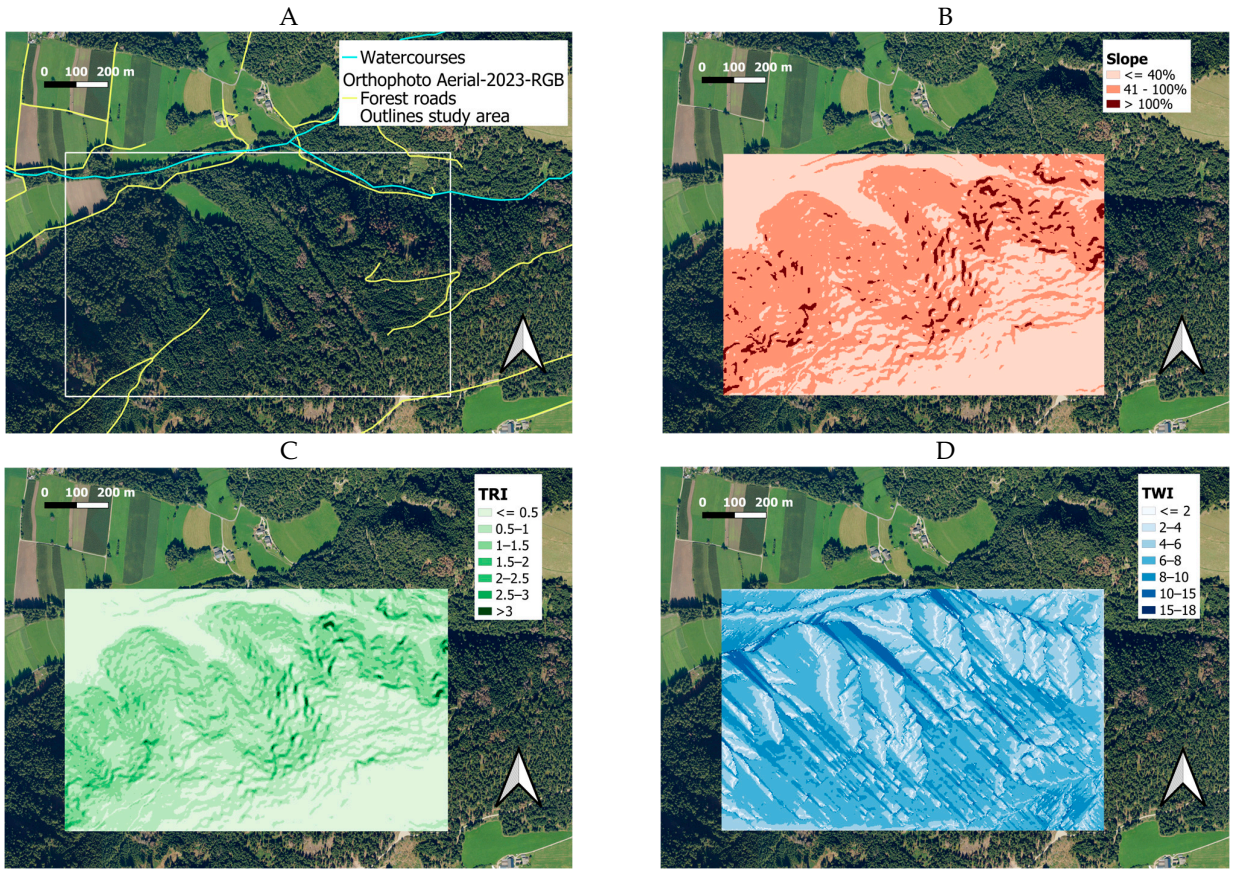

Figure 3. The collective of the layers representing the operational criteria for the most suitable harvesting machine configuration: forest roads and watercourses (**A**), slope (**B**), topographic ruggedness index (TRI) (**C**), and Topographic Wetness Index (TWI) (**D**).

3.2. The Layer Determining the Silvicultural Conditions (DBH Classes)

Step 1: Setting up the DeepForest algorithm

The tree crowns identified by the model before and after fine-tuning are shown in Figure 4A and Figure 4B, respectively. The ground truth, as delineated by hand, is shown in Figure 4C. Figure 4D displays a different subsection, illustrating the results of tree crown detection using the fine-tuned DeepForest model. In this case, the tree crowns are not highlighted, but the tree tops are.

The fine-tuning of the DeepForest algorithm resulted in the following accuracy in terms of the F1 score: Precision of the pre-trained, as well as of the fine-tuned, model is notably higher than Recall, highlighting that the algorithm makes fewer errors in predicting trees where none exist (false positives) than in failing to identify actual trees (false negatives, i.e., overlooked trees). The F1 of the fine-tuned model (F1 = 0.794) is slightly better than that of the pre-trained model (F1 = 0.752). Therefore, the former was adopted.

When applied to the orthophoto of the experimental area, the DeepForest algorithm identified 147 trees per hectare, compared to the actual stem count of 350 trees (above a threshold diameter of 10 cm). The algorithm predicted no false positives, meaning that, in all the cases where the algorithm identified a tree, there was a tree. In contrast, the algorithm produced 58% false negatives, which represents the share of overlooked trees. Thus, the F1 score of the fine-tuned model, when tested against field observation, is 0.60. Table 2 presents the accuracy results from the fine-tuning process of the DeepForest algorithm, as well as the performance of the fine-tuned model when applied to detect trees across the test area.

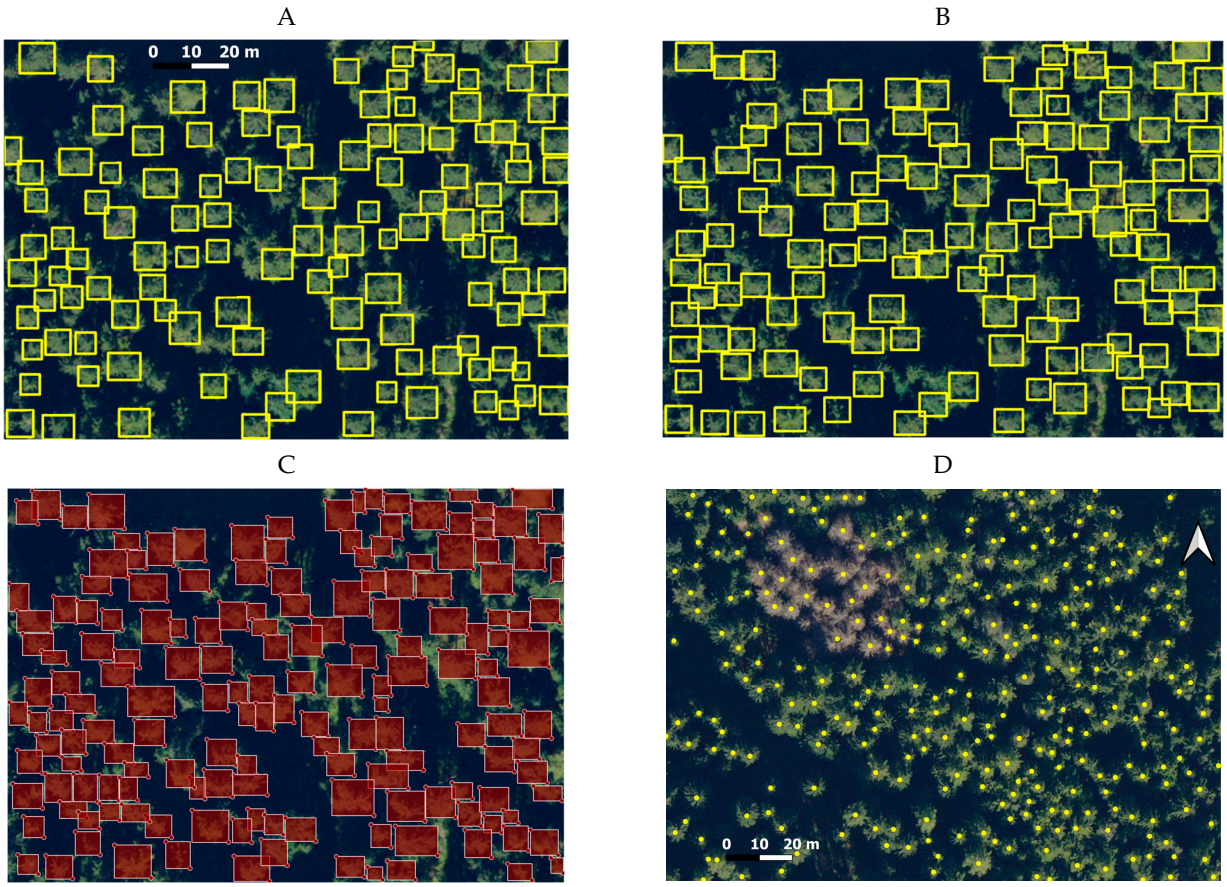

Figure 4. Subsections of the study area for calibrating the DeepForest model. (**A**) Pre-trained model; (**B**) fine-tuned model; and (**C**) ground truth; (**D**) shows a separate section after tree crown prediction by the fine-tuned model.

Table 2. Performance of the DeepForest algorithm, pre-trained and fine-tuned, against the ground truth, as shown in Figure 4C, and performance of the calibrated model against field survey results.

	Predicted		**Ground Truth**
Fine-tuning the model	Pre-trained	Fine-tuned	
Nr of trees as in Figure 4C	118	122	166
Precision	0.899	0.913	
Recall	0.649	0.703	
F1	0.752	0.794	
Prediction performance			
Nr of trees (observed per hectare)	147		350
Precision	1.00		
Recall	0.429		
F1	0.600		

Step 2: Deriving tree diameters by allometric functions

The data structure of the tree diameters calculated by the three allometric equations (Equations (1)–(3)) is illustrated in Figure 5. The calculated diameters are contrasted by the observed values. Figure 5 (left-hand side) shows the histograms, while Figure 5 (right-hand side) shows the point–line plots for the differences between predicted and observed values.

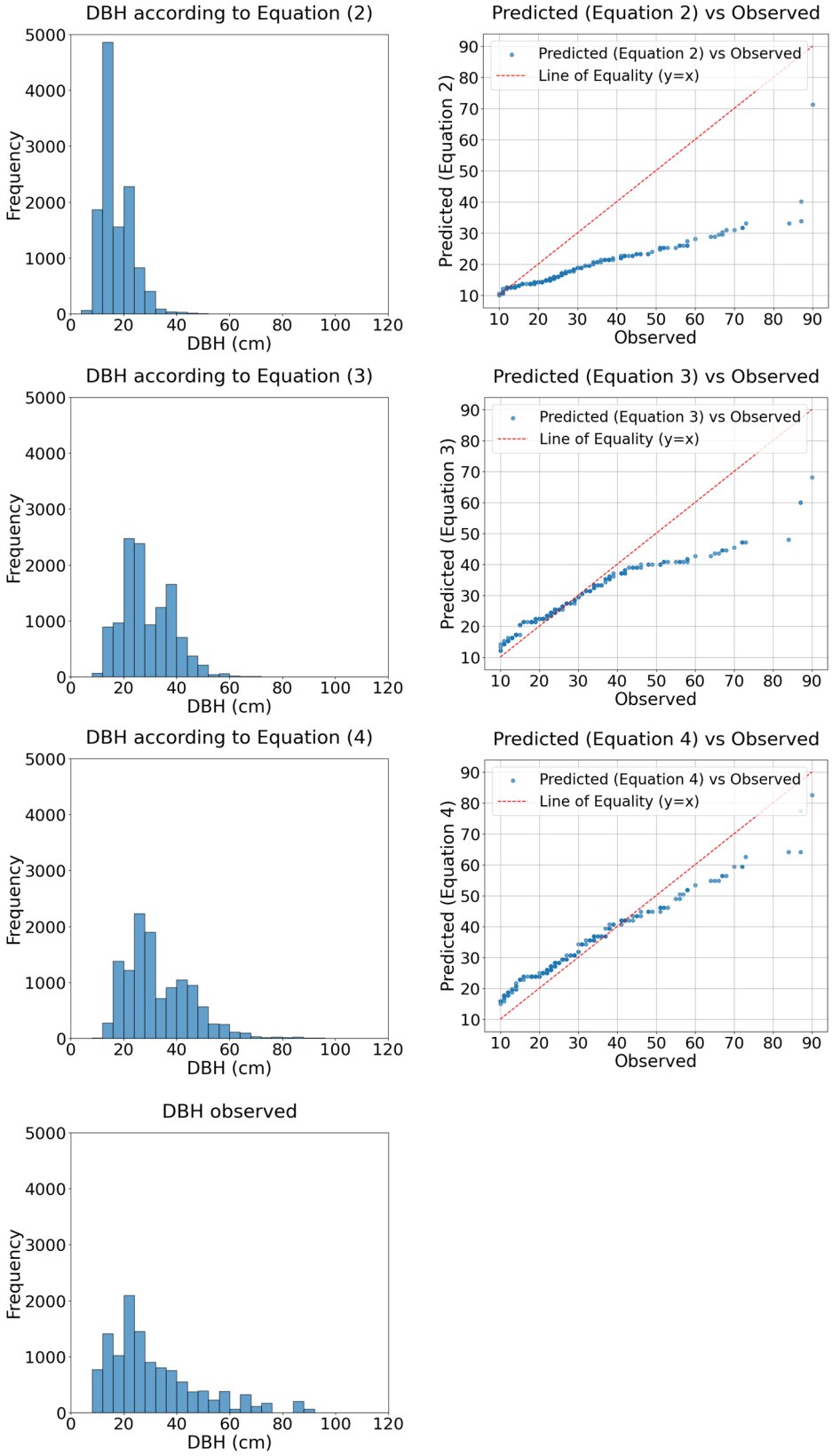

Figure 5. Data structure of the theoretical and observed values for DBH (**left-hand side**), and point–line plots for the residuals when subtracting the observed from the calculated DBH values (**right-hand side**).

Table 3 provides descriptive statistics for calculated and observed DBH and height values, including the distribution of frequencies across DBH classes. Additionally, it

details the calculated metrics (Pearson's R^2, Anderson–Darling test/AD, mean absolute error/MAE, mean bias error/MBE, normalized root mean square error/NRMSE), comparing the predicted DBH against the observed DBH.

Table 3. Comparison of theoretically derived and observed values for DBH and tree height. CHM stands for Canopy Height Model, AD for Anderson–Darling test, MAE for mean absolute error, MBA for mean bias error, and NRMSE for normalized root mean square error. For the comparison of the DBH classes, the predicted data (n = 12,472) were proportionally scaled down to match the number of trees observed on the ground (n = 196). Since, on the ground, only the median heights of the sample plots (height of the tree with the median diameter) were measured, the values for the minimum and the maximum are not listed.

	DBH (cm)				Height (m)	
Value	**Equation (2)**	**Equation (3)**	**Equation (4)**	**Observed**	**CHM**	**Observed**
Count	12,472	12,472	12,472	196	12,472	28
Mean	17.097	28.608	33.245	31.929	22.479	24.565
Std	6.111	9.630	12.839	12.327	7.050	6.788
Min	6.019	7.407	10.789	14.975	5.376	
50%	15.330	26.408	29.435	28.276	22.807	24.000
Max	76.221	89.981	164.657	95.310	49.203	
DBH 10–20	130 (66%)	31 (16%)	27 (14%)	56 (29%)		
DBH 21–50	65 (33%)	162 (82%)	149 (76%)	112 (57%)		
DBH > 50	1 (1%)	3 (2%)	20 (10%)	28 (14%)		
R^2	0.873	0.948	0.984			
AD	0.001	0.001	0.001			
MAE	12.426	4.784	4.566			
MBE	−12.381	−2.318	1.742			
NRMSE	0.207	0.102	0.069			

The Anderson–Darling test indicates that all three calculated groups (Equations (1)–(3)) originate from significantly different distributions than the observed values ($p < 0.05$). This suggests that, despite high correlation coefficients (R^2), these variables exhibit systematic deviations at increases in the values. This finding underlines the importance of evaluating model agreement beyond correlation alone, suggesting the necessity of error metrics (MAE, MBE, and NRMSE) to quantify absolute differences. Among the models, Equation (4) achieves the highest accuracy in terms of the error metrics (MAE = 4.566, MBE = 1.742, NRMSE = 0.069), demonstrating the best alignment with the observations.

Step 3: Mapping the diameter classes across the study area

Consequently, Equation (4) was integrated in the predictive model, and the third work step for generating the silvicultural layer was completed. Figure 6 represents the spatial distribution of the tree diameters across the study site.

According to Figure 6, the diameter class of 11–20 cm covers 11%, the diameter class of 21–50 cm covers 74%, and the diameter class > 50 cm covers 15% of the forested area.

The validation results of the predictive model for TRI, TWI, and diameter class patches are listed in Table 4.

Overall, the model accurately predicted trafficability for ruggedness (TRI) in 26 out of 28 cases (93%), for soil-bearing capacity (TWI) in 24 out of 28 cases (86%), and for DBH class in 21 out of 28 instances (75%).

For illustration purposes, three test runs were conducted with the generated model, varying the values for TRI and TWI to explore different management preferences. In the first run, forest managers were assumed to prioritize ground-based equipment and to show less concern for environmental impacts, thus permitting machine operation up to a TRI of 2 and a TWI of 10. The result of this scenario is depicted in Figure 7A. In the second run and the third run, forest managers were assumed to have a more restrictive approach,

giving more importance to reduced environmental impact. For the second run (Figure 7B), a maximum allowable TRI of 1 and a TWI of 10 were assumed. In the third run (Figure 7C), the parameters were set to a TRI of 2 and a TWI of 5.

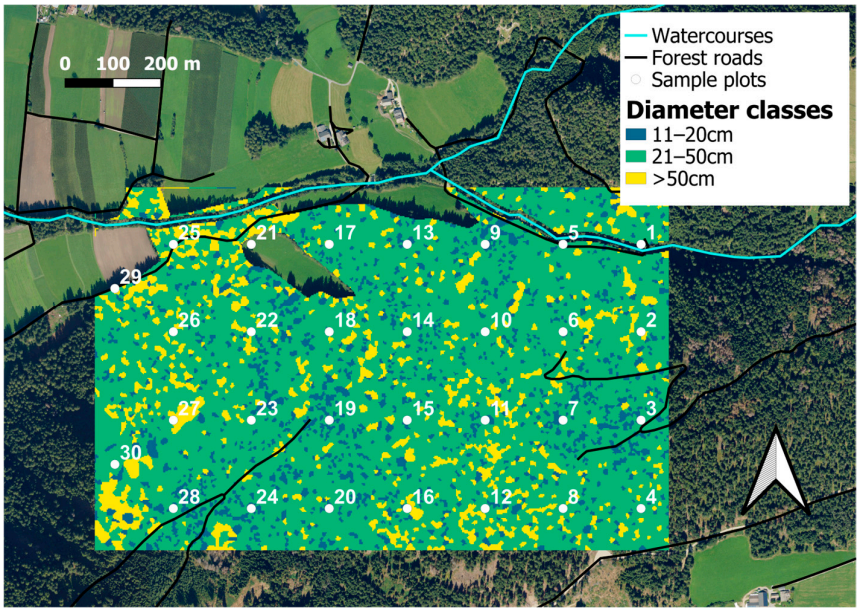

Figure 6. Spatial distribution of the diameter classes of the experimental area, as determined by the Inverse Distance Weighting (IDW) interpolation algorithm.

Table 4. Validation results of the generated model. A match is found if the model prediction aligns with the respective observation on site (see explanations in the text).

	TRI Match Summary		**TWI Match Summary**	
	Model outcome	Count	Model outcome	Count
	Match	26	Match	24
	Mismatch	2	Mismatch	4
	DBH Class Confusion Matrix			
		Predicted		
		Small	Medium	Large
Observed	Small	3	1	0
	Medium	1	15	1
	Large	1	3	3

As can be seen from Figure 7, ground-based equipment operates exclusively within the pre-defined 200 m proximity to forest roads and beyond the 10 m buffer zone on either side of existing watercourses. Additionally, areas with slopes exceeding 150% remain unharvested, as indicated by the spots displaying the bare orthophoto colors. When setting the TRI to 2 and the TWI to 10, the zone inside the 200 m zone can be almost entirely operated by ground-based equipment (Figure 7A). At reductions in threshold for TRI and TWI, the share of ground-based logging is noticeably reduced. Table 5 displays the numerical outcomes of the three demonstrated scenarios.

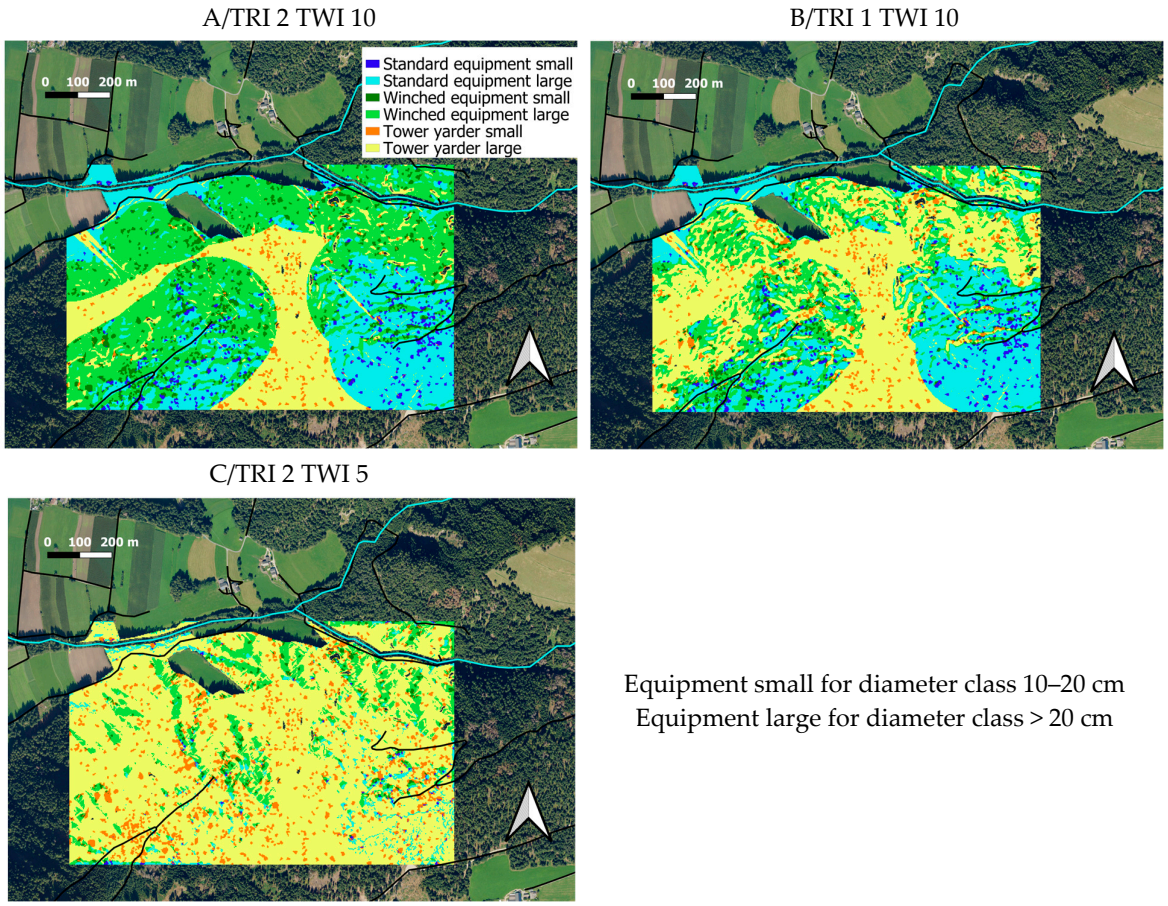

Figure 7. Three test runs with the generated GIS-based Decision Support Model, reflecting various pre-defined operational constraints: (**A**) less restrictive scenario favoring ground-based equipment; (**B**) more restrictive scenario with lower TRI; (**C**) scenario prioritizing wetness constraints with lower TWI. Standard equipment denotes the standard ground-based machinery, harvester–forwarder, Winched equipment refers to the winch-assisted harvester and forwarder, and Tower yarder is the machinery used for cable logging. All maps in this figure are based on the same 2023 orthophoto (source: South Tyrolean Citizen Network, Mapview Portal), shown in Figure 2.

Table 5. Percentages of the area harvestable by different machine configurations (see Figure 7). *St* means standard equipment, *Wi* means winched equipment, *Ty* means tower yarder, *s* stands for small and *l* stands for large. *No h* denotes areas that are not harvestable (above 150% slope).

Scenario	St s	St l	Wi s	Wi l	Ty s	Ty l	No h	Total
TRI 2 TWI10	3	24	5	37	2	19	10	100
TRI 1 TWI10	3	24	3	18	4	38	10	100
TRI 2 TWI 5	1	3	1	9	8	68	10	100

In the first scenario (Figure 7A), the percentage of ground-based logging is 69%, and of cable-based logging, 21% (Table 5). In the second scenario (Figure 7B), the areas suitable for ground-based machinery decrease to 48%, whereas those suitable for cable- logging increase to 42% (Table 5). Finally, in scenario three (Figure 7C), ground-based logging drops to 14%, and cable-based logging climbs to 76% (Table 5).

4. Discussion

4.1. Operational Predictions of the Model

Our Decision Support Model effectively assesses terrain trafficability, since the model's predictions for the test area aligned well with ground observations (Table 4). These pre-

dictions were based on two key parameters: the Topographic Wetness Index (TWI), which evaluates soil moisture and vulnerability to machine traffic using spatial data, and the Topographic Ruggedness Index (TRI), which measures terrain ruggedness by calculating elevation changes between grid cells.

In the context of this study, the TWI turned out to be a highly sensitive and effective measure, since the substantial impact of the TWI on the applicability of ground-based logging was demonstrated (Figure 7, Table 5). The TWI is considered a useful tool with which to assess soil conditions and to predict trafficability for forest operations [52]. Still, it is suggested not to be used in isolation for logging operations. Instead, it should be combined with additional data sources, such as soil maps, forest inventory records, hydrological models, weather data, and real-time machine data, if available [53]. Similarly, it is recommended to use the TRI with additional soil-related data. However, TWI and TRI, when combined with each other (as they were in the present study) can improve terrain classification and enhance trafficability assessments [54]. This resonates with the principal aim of this study, i.e., to develop a low-budget tool based on easily accessible data sources, as represented by a Digital Terrain Model (DTM), based on which both indicators can be derived.

Our model, therefore, is a valuable tool for achieving an overview on the operational conditions of a woodlot. However, for detailed operational planning, it does not replace on-site inspections or the use of additional information to obtain a more comprehensive understanding of the site conditions.

4.2. Silvicultural Predictions of the Model

4.2.1. Setting up the DeepForest Algorithm

The validation of the tree detection algorithm DeepForest for the purpose of this study was completed in two steps: firstly, based on the ground truth, as outlined on the related orthophoto section; and secondly, based on the ground truth gained by field survey (Figure 4C, Table 2). The first step of validation showed an F1-score of 0.79, while the second showed an F1-score of 0.60 (Table 2). This result is comparable to the findings of [20], who, likewise, used plane-based aerial imagery with a CNN neural network for tree detection, achieving an average F1-score of 0.76 (based on ground truth as outlined on an orthophoto section). When compared to studies using UAV-based RGB imagery, such as [13,14], who reported F1-scores above 0.80, it becomes clear that UAV-based imagery provides higher precision due to its higher resolution. UAV studies integrating LiDAR data, such as [18], have exhibited even better accuracy (F1-scores up to 0.85), highlighting the advantages of combining RGB and 3D structural information for tree crown detection. These comparisons suggest that, while plane-based RGB imagery (orthophoto) is effective for large-scale tree detection, higher-resolution UAV data and LiDAR inputs can significantly improve accuracy.

4.2.2. Generating the Map on Diameter Class Distribution

The creation of the silvicultural layer was a key focus of this study. This layer illustrates the distribution of tree growth classes across the area (Figure 6). The model demonstrated convincing accuracy, correctly predicting the diameter class for 21 out of 28 sample plots (Table 4), confirming its reliability in assessing stand structure.

From a silvicultural perspective, this layer provides an overview of current growth patterns in the study area. The map shows that 74% of the forest consists of trees in the 21–50 cm diameter class, followed by 15% exceeding 50 cm, and 11% in the 11–20 cm class (Figure 6). According to [55], this distribution indicates a predominant maturation stage with biomass accumulation, as well as structural diversification in older trees.

The created spatial map helps forest managers locate growth class patches and assess machinery suitability at the same time (Figures 6 and 7, Table 5). By integrating growth data with data on operational constraints, managers can optimize harvesting logistics and adjust strategies as needed. This way, the model serves in both regards, as a diagnostic tool for the current state, and as a guide for future management decisions.

4.3. Model Limitations

To ensure a balanced perspective, we also want to underscore the limitations of the presented Decision Support Model.

Currently, the DeepForest algorithm, when applied to orthophoto imagery, struggles to accurately distinguish between tree species, since it is primarily trained for tree crown delineation, rather than species classification [30]. As a result, our study had to generalize tree species based on the dominant species of the test area.

Another limitation is that the algorithm, when compared to ground-collected data, significantly underestimates the total number of trees, missing a substantial portion by a margin of 58% (Table 2). As mentioned above, this tendency of DeepForest to overlook smaller trees has also been observed in [16].

However, a more detailed examination of these findings is essential. We can only state with certainty that the DeepForest algorithm overlooks a certain number of trees, but we cannot be certain if most of these overlooked trees are in the lower or upper end of the size distribution. This uncertainty persists even if we contrast the predicted numbers with ground-collected data, since we cannot directly compare crowns identified by the algorithm with those observed on the ground. Instead, we can only compare diameters calculated (allometric functions) from predicted crowns (DeepForest algorithm) to diameters measured on the ground. Errors in the predicted diameters could arise from two sources: limitations in the tree detection algorithm, or flaws in the allometric function used to estimate diameters. For example, using Equation (2), there seems to be no shortage of small trees (Table 3). But, when considering the overall distribution of tree diameters, Equation (4) appears to provide the smoothest results. It predicts a balanced distribution of small, medium, and large trees in good alignment with the observed values. Assuming that Equation (4) is the most accurate one, out of the three functions tested, our method predicts fewer small trees (14% versus the 29% observed) and fewer large trees (10% versus the 14% observed) (Table 3). The underestimation of small trees is likely due to the tree detection algorithm failing to detect them when they are hidden beneath the canopy's top layer.

Conversely, the underestimation of large trees may also stem from the limitations of the allometric function. This limitation arises because tree growth patterns differ as trees age. At a certain age, a tree's height growth slows down, while its diameter growth can accelerate [56,57]. Additionally, crown expansion is more closely related to height growth [58] than to diameter growth, since trees grow taller primarily to expand their crowns. Once crown growth stabilizes, diameter growth continues, leading to underestimation by functions that calculate diameter based on crown size [59].

Thus, as a combination of DeepForest and Equation (4), our methodology indicates a slight bias in the estimations across the diameter classes (Figure 5, Table 3). However, when looking at the overall performance of the model, the results are promising. The mean absolute error (MAE) and the average percentage deviation relative to the total diameter range (NMRSE) (Table 3) demonstrate reasonable accuracy for practical applications.

The accuracy of predictions made by algorithms such as DeepForest is subject to a certain degree of variability, which arises from multiple factors, including the following: the type of forest being analyzed; its density; its species diversity; and its structural complexity [60]. Among these, one of the most critical factors is the quality of the input

dataset. High-quality, up-to-date datasets are essential for the algorithm to produce reliable and actionable outputs. It is reasonable to anticipate that the performance of such algorithms will continue to improve over time, driven by advancements in technology and data acquisition methods. In our study, for instance, we observed a significant increase in prediction accuracy when we used the orthophotos from 2023, compared to those from 2020. This improvement underscores the importance of leveraging the latest available datasets, as newer imaging technologies and higher-resolution data can better capture the subtle variations in forest structure, ultimately enhancing the algorithm's output.

4.4. Perspectives on the Model as a Decision Support Tool and Its Future Development

Importantly, the decision support by the here-presented model is not provided by a procedural (black box) algorithm that runs based on hidden rules, but is provided in a visual format. The generated maps serve as the interface for decision making, as each pixel displays both operability (based on slope, ruggedness, wetness, and road proximity) and stand maturity (based on DBH class). This allows forest managers to visually interpret, at a glance, which areas are suited for different harvesting systems and which silvicultural interventions (e.g., pre-commercial thinning vs. final harvest) could be performed.

To implement this system more broadly, two approaches are conceivable. The first involves creating an interactive geoportal, integrated, e.g., in the *Mapview Portal* of the South Tyrolean Citizen Network [49]. For a given region, multiple layers could be made available, each representing different configurations of harvesting systems based on pre-set values for slope, ruggedness, and soil resistance thresholds. The second option is a mobile application (App) that users can download on their cell phones. This would offer greater interactivity, allowing users to interactively adjust settings, enabling them to define parameters like diameter class thresholds, maximum machine-operable slopes, critical ruggedness values (TRI), and adjustments for soil bearing capacity (TWI). This flexibility would accommodate varying priorities, such as balancing low-impact measures with economic optimization.

5. Conclusions

This study developed a map-based Decision Support Model (DSM) that enables harvesting system selection on sloping terrain. The model was implemented using conditional GIS logic that overlays constraints such as harvesting exclusion zones, forest road networks, and slope, as well as Topographic Ruggedness (TRI) and Topographic Wetness (TWI) Indexes to assess maneuverability, while tree detection was performed using the DeepForest algorithm, and tree diameters were estimated through allometric functions.

Validation results showed that the model predicted trafficability and stand maturity with accuracies of 93% (TRI), 86% (TWI), and 75% (DBH class). Even though the model provided a reliable spatial representation of tree size classes, it underestimated the total number of trees, particularly smaller trees, in comparison to field data—a flaw likely connected to the crown detection ability of the DeepForest algorithm. Nevertheless, the model shows good performance in integrating operational and silvicultural criteria into spatial decision layers, and in simulating different management scenarios.

To improve the model, further training of the tree detection algorithm could enhance the identification of tree species, as well as of smaller trees, and further quality improvement of the orthophoto imagery could refine crown recognition, specifically of smaller trees.

All software used in this study is open-source and freely downloadable (GRASS GIS, QGIS, SAGA GIS, and Python with the DeepForest neural network). The analyses were conducted on a standard workstation with 16 GB RAM and a quad-core processor, which was sufficient for all tasks in terms of spatial processing and model execution. No infrastructure for high-performance computing was needed.

It is important to note that this study aimed at the scientific conceptualization and testing of the model, not at its engineering implementation. The modular structure of the current model allows interested users to reproduce each step of our workflow manually. Full integration into a coherent tool constitutes a logical next step, but lies beyond the scope of this proving-the-concept research. Simplifying the workflow and integrating all here-applied methods into a single-interface, user-friendly tool, such as an application ready for download, could greatly support forest management planning.

Author Contributions: Conceptualization, B.E., Z.T. and R.S.; Methodology, B.E., Z.T., N.M. and R.S.; Software, B.E.; Validation, B.E.; Formal analysis, B.E.; Investigation, B.E.; Resources, B.E., N.M. and R.S.; Data curation, B.E., N.M. and R.S.; Writing—original draft, B.E., Z.T., N.M. and R.S.; Writing—review & editing, B.E., Z.T., N.M. and R.S.; Visualization, B.E.; Supervision, R.S.; Project administration, R.S.; Funding acquisition, R.S. All authors have read and agreed to the published version of the manuscript.

Funding: This research received no external funding.

Data Availability Statement: Data are contained within the article.

Conflicts of Interest: The authors declare no conflict of interest.

References

1. Jordan, P.; Millard, T.H.; Campbell, D.; Schwab, J.W.; Wilford, D.J.; Nicol, D.; Collins, D. Forest management effects on hillslope processes. *Compend. For. Hydrol. Geomorphol. Br. Columbia. BC Min. For. Range* **2010**, *66*, 275.
2. Visser, R.; Stampfer, K. Expanding ground-based harvesting onto steep terrain: A review. *Croat. J. For. Eng. J. Theory Appl. For. Eng.* **2015**, *36*, 321–331.
3. Spinelli, R.; Cacot, E.; Mihelic, M.; Nestorovski, L.; Mederski, P.; Tolosana, E. Techniques and productivity of coppice harvesting operations in Europe: A meta-analysis of available data. *Ann. For. Sci.* **2016**, *73*, 1125–1139. [CrossRef]
4. Holzfeind, T.; Visser, R.; Chung, W.; Holzleitner, F.; Erber, G. Development and Benefits of Winch-Assist Harvesting. *Curr. For. Rep.* **2020**, *6*, 201–209. [CrossRef]
5. Schweier, J.; Ludowicy, C. Comparison of A Cable-Based and a Ground-Based System in Flat and Soil-Sensitive Area: A Case Study from Southern Baden in Germany. *Forests* **2020**, *11*, 611. [CrossRef]
6. Bont, L.G.; Fraefel, M.; Frutig, F.; Holm, S.; Ginzler, C.; Fischer, C. Improving forest management by implementing best suitable timber harvesting methods. *J. Environ. Manag.* **2022**, *302*, 114099. [CrossRef]
7. Erber, G.; Spinelli, R. Timber extraction by cable yarding on flat and wet terrain: A survey of cable yarder manufacturer's experience. *Silva Fenn.* **2020**, *54*, 10211. [CrossRef]
8. Sundberg, B.; Silversides, C.R. *Operational Efficiency in Forestry: Vol. 1: Analysis. Vol. 29*; Springer Science & Business Media: Berlin/Heidelberg, Germany, 1988. [CrossRef]
9. Piragnolo, M.; Grigolato, S.; Pirotti, F. Planning harvesting operations in forest environment: Remote sensing for decision support. In *ISPRS Annals of Photogrammetry, Remote Sensing and Spatial Information Sciences*; Copernicus GmbH: Göttingen, Germany, 2019; pp. 33–40. [CrossRef]
10. Mederski, P.S.; Werk, K.; Bembenek, M.; Karaszewski, Z.; Brunka, M.; Naparty, K. Harvester efficiency in trunk utilisation and log quality of early thinning pine trees. *For. Res. Pap.* **2019**, *80*, 45–53. [CrossRef]
11. Spinelli, R.; Magagnotti, N. Comparison of two harvesting systems for the production of forest biomass from the thinning of *Picea abies* plantations. *Scand. J. For. Res.* **2010**, *25*, 69–77. [CrossRef]
12. Gan, Y.; Wang, Q.; Iio, A. Tree Crown Detection and Delineation in a Temperate Deciduous Forest from UAV RGB Imagery Using Deep Learning Approaches: Effects of Spatial Resolution and Species Characteristics. *Remote Sens.* **2023**, *15*, 778. [CrossRef]
13. Fu, H.; Zhao, H.; Jiang, J.; Zhang, Y.; Liu, G.; Xiao, W.; Du, S.; Guo, W.; Liu, X. Automatic detection tree crown and height using Mask R-CNN based on unmanned aerial vehicles images for biomass mapping. *For. Ecol. Manag.* **2024**, *555*, 121712. [CrossRef]
14. Zhang, C.; Zhou, J.; Wang, H.; Tan, T.; Cui, M.; Huang, Z.; Wang, P.; Zhang, L. Multi-Species Individual Tree Segmentation and Identification Based on Improved Mask R-CNN and UAV Imagery in Mixed Forests. *Remote Sens.* **2022**, *14*, 874. [CrossRef]
15. Sivanandam, P.; Lucieer, A. Tree Detection and Species Classification in a Mixed Species Forest Using Unoccupied Aircraft System (UAS) RGB and Multispectral Imagery. *Remote Sens.* **2022**, *14*, 4963. [CrossRef]
16. Persson, D. *Tree Crown Detection Using Machine Learning: A Study on Using the DeepForest Deep-Learning Model for Tree Crown Detection in Drone-Captured Aerial Footage*; KTH Royal Institute of Technology: Stockholm, Sweden, 2024.

17. Wang, Z.; Li, P.; Cui, Y.; Lei, S.; Kang, Z. Automatic Detection of Individual Trees in Forests Based on Airborne LiDAR Data with a Tree Region-Based Convolutional Neural Network (RCNN). *Remote Sens.* **2023**, *15*, 1024. [CrossRef]
18. Bennett, L.; Wilson, B.; Selland, S.; Qian, L.; Wood, M.; Zhao, H.; Boisvert, J. Image to attribute model for trees (ITAM-T): Individual tree detection and classification in Alberta boreal forest for wildland fire fuel characterization. *Int. J. Remote Sens.* **2022**, *43*, 1848–1880. [CrossRef]
19. Freudenberg, M.; Schnell, S.; Magdon, P. A Sentinel-2 machine learning dataset for tree species classification in Germany. *Earth Syst. Sci. Data Discuss.* **2024**, *2024*, 1–20. [CrossRef]
20. Beloiu, M.; Heinzmann, L.; Rehush, N.; Gessler, A.; Griess, V.C. Individual Tree-Crown Detection and Species Identification in Heterogeneous Forests Using Aerial RGB Imagery and Deep Learning. *Remote Sens.* **2023**, *15*, 1463. [CrossRef]
21. Klosterhuber, R.; Plettenbacher, T. *Vorrangige Holzernteverfahren auf der Technisch Nutzbaren Waldfläche in Südtirol und Ihre Tauglichkeit für Vollbaumnutzung*; Report Commissioned by TIS Innovation Park; WLM Büro für Vegetationsökologie und Umweltplanung Klosterhuber & Partner OG: Bolzano, Italy, 2013.
22. Phelps, K.; Hiesl, P.; Hagan, D.; Hagan, A.H. The Harvest Operability Index (HOI): A Decision Support Tool for Mechanized Timber Harvesting in Mountainous Terrain. *Forests* **2021**, *12*, 1307. [CrossRef]
23. QGIS Development Team. *QGIS Geographic Information System*; Open Source Geospatial Foundation: Chicago, IL, USA, 2018. Available online: https://qgis.org (accessed on 15 October 2024).
24. Conrad, O.; Bechtel, B.; Bock, M.; Dietrich, H.; Fischer, E.; Gerlitz, L.; Wehberg, J.; Wichmann, V.; Böhner, J. System for Automated Geoscientific Analyses (SAGA) v. 2.1.4. *Geosci. Model Dev.* **2015**, *8*, 1991–2007. [CrossRef]
25. GRASS Development Team. *Geographic Resources Analysis Support System (GRASS GIS) Software*, v. 8; Open Source Geospatial Foundation: Beaverton, OR, USA, 2024. Available online: https://grass.osgeo.org (accessed on 15 October 2024).
26. Visser, R.; Spinelli, R. *Assessment of a Winch-Assisted Skidder in Castle Downs Forest, New Zealand*; Rep H048 For Grow Res Ltd.: Rotorua, New Zealand, 2020.
27. Engler, B.; Hartmann, G.; Mederski, P.S.; Bont, L.G.; Picchi, G.; Alcoverro, G.; Purfürst, T.; Schweier, J. Impact of Forest Operations in Four Biogeographical Regions in Europe: Finding the Key Drivers for Future Development. *Curr. For. Rep.* **2024**, *10*, 337–359. [CrossRef]
28. Riley, S.J.; DeGloria, S.D.; Elliot, R. Index that quantifies topographic heterogeneity. *Intermt. J. Sci.* **1999**, *5*, 23–27.
29. Beven, K.J.; Kirkby, M.J. A physically based, variable contributing area model of basin hydrology/Un modèle à base physique de zone d'appel variable de l'hydrologie du bassin versant. *Hydrol. Sci. J.* **1979**, *24*, 43–69. [CrossRef]
30. Weinstein, B.G.; Marconi, S.; Aubry-Kientz, M.; Vincent, G.; Senyondo, H.; White, E.P. DeepForest: A Python package for RGB deep learning tree crown delineation. *Methods Ecol. Evol.* **2020**, *11*, 1743–1751. [CrossRef]
31. Russell, B.C.; Torralba, A.; Murphy, K.P.; Freeman, W.T. LabelMe: A Database and Web-Based Tool for Image Annotation. *Int. J. Comput. Vis.* **2008**, *77*, 157–173. [CrossRef]
32. Rijsbergen, V. Reviews: Van Rijsbergen, C.J. Information retrieval. 2nd edn. London, Butterworths, I978. 208pp. *J. Librariansh.* **1979**, *11*, 237. [CrossRef]
33. Hasenauer, H. Dimensional relationships of open-grown trees in Austria. *For. Ecol. Manag.* **1997**, *96*, 197–206. [CrossRef]
34. Jucker, T.; Caspersen, J.; Chave, J.; Antin, C.; Barbier, N.; Bongers, F.; Dalponte, M.; van Ewijk, K.Y.; Forrester, D.I.; Haeni, M.; et al. Allometric equations for integrating remote sensing imagery into forest monitoring programmes. *Glob. Change Biol.* **2017**, *23*, 177–190. [CrossRef]
35. Pretzsch, H.; Biber, P.; Ďurský, J. The single tree-based stand simulator SILVA: Construction, application and evaluation. *For. Ecol. Manag.* **2002**, *162*, 3–21. [CrossRef]
36. Gauthier, M.-M.; Tremblay, S. Precommercial thinning as a silvicultural option for treating very dense conifer stands. *Scand. J. For. Res.* **2018**, *33*, 446–454. [CrossRef]
37. Simard, S.W.; Blenner-Hassett, T.; Cameron, I.R. Pre-commercial thinning effects on growth, yield and mortality in even-aged paper birch stands in British Columbia. *For. Ecol. Manag.* **2004**, *190*, 163–178. [CrossRef]
38. Saari, V.; Peura, M.; Halme, P. Effects of changed interpretation of the Finnish Forest Act on the Riparian Woodland Key habitats. *Scand. J. For. Res.* **2024**, *39*, 377–391. [CrossRef]
39. Marchi, E.; Picchio, R.; Spinelli, R.; Verani, S.; Venanzi, R.; Certini, G. Environmental impact assessment of different logging methods in pine forests thinning. *Ecol. Eng.* **2014**, *70*, 429–436. [CrossRef]
40. Picchio, R.; Mederski, P.S.; Tavankar, F. How and How Much, Do Harvesting Activities Affect Forest Soil, Regeneration and Stands? *Curr. For. Rep.* **2020**, *6*, 115–128. [CrossRef]
41. Leslie, C. Productivity and Utilisation of Winch-Assist Harvesting Systems: Case Studies in New Zealand and Canada. Master's Thesis, University of Canterbury, Christchurch, New Zealand, 2019.
42. Marchi, L.; Grigolato, S.; Mologni, O.; Scotta, R.; Cavalli, R.; Montecchio, L. State of the Art on the Use of Trees as Supports and Anchors in Forest Operations. *Forests* **2018**, *9*, 467. [CrossRef]

43. Obi, F.; Visser, R. *Benchmarking 2019 Data and Longer-Term Productivity and Cost Analyses*; Technical Report; School of Forestry, University of Canterbury: Christchurch, New Zealand, 2020.
44. Pourali, S.H.; Arrowsmith, C.; Chrisman, N.; Matkan, A.A.; Mitchell, D. Topography Wetness Index Application in Flood-Risk-Based Land Use Planning. *Appl. Spat. Anal. Policy* **2016**, *9*, 39–54. [CrossRef]
45. Abetz, P. Eine Entscheidungshilfe für die Durchforstung von Fichtenbeständen. *Allg Forstz.* **1975**, *30*, 666–667.
46. GRASS Development Team. r.mapcalc—GRASS GIS Manual. Available online: https://grass.osgeo.org/grass82/manuals/r.mapcalc.html (accessed on 15 October 2024).
47. Anderson, T.W.; Darling, D.A. Asymptotic Theory of Certain "Goodness of Fit" Criteria Based on Stochastic Processes. *Ann. Math. Stat.* **1952**, *23*, 193–212. [CrossRef]
48. James, G.; Witten, D.; Hastie, T.; Tibshirani, R. *An Introduction to Statistical Learning*; Springer: Berlin/Heidelberg, Germany, 2013; p. 9.
49. South Tyrolean Citizen Network. Mapview Portal. Available online: https://mapview.civis.bz.it (accessed on 15 October 2024).
50. Autonomous Province of Bolzano. Office for Meteorology and Avalanche Warning: Climate Data Portal. Available online: https://wetter.provinz.bz.it/download-messdaten.asp (accessed on 26 February 2025).
51. Python Software Foundation. *Python*, Version 3.11.7; Python Software Foundation: Delaware, DE, USA, 2023. Available online: https://www.python.org (accessed on 15 October 2024).
52. Hoffmann, S.; Schönauer, M.; Heppelmann, J.; Asikainen, A.; Cacot, E.; Eberhard, B.; Hasenauer, H.; Ivanovs, J.; Jaeger, D.; Lazdins, A.; et al. Trafficability Prediction Using Depth-to-Water Maps: The Status of Application in Northern and Central European Forestry. *Curr. For. Rep.* **2022**, *8*, 55–71. [CrossRef]
53. Salmivaara, A.; Launiainen, S.; Perttunen, J.; Nevalainen, P.; Pohjankukka, J.; Ala-Ilomäki, J.; Sirén, M.; Laurén, A.; Tuominen, S.; Uusitalo, J.; et al. Towards dynamic forest trafficability prediction using open spatial data, hydrological modelling and sensor technology. *For. Int. J. For. Res.* **2020**, *93*, 662–674. [CrossRef]
54. Cao, S. Soil rutting prediction using Random Forest model. *For. Ecol. Manag.* **2024**, *558*, 121361.
55. Franklin, J.F.; Spies, T.A.; Van Pelt, R.; Carey, A.B.; Thornburgh, D.A.; Berg, D.R.; Lindenmayer, D.B.; Harmon, M.E.; Keeton, W.S.; Shaw, D.C.; et al. Disturbances and structural development of natural forest ecosystems with silvicultural implications, using Douglas-fir forests as an example. *For. Ecol. Manag.* **2002**, *155*, 399–423. [CrossRef]
56. Fabris, S. Influence of Cambial Ageing, Initial Spacing, Stem Taper and Growth Rate on the Wood Quality of Three Coastal Conifers. Master's Thesis, University of British Columbia, Vancouver, BC, Canada, 2000.
57. Larson, B.C. Development and growth of even-aged stands of Douglas-fir and grand fir. *Can. J. For. Res.* **1986**, *16*, 367–372. [CrossRef]
58. Begović, K.; Schurman, J.S.; Svitok, M.; Pavlin, J.; Langbehn, T.; Svobodová, K.; Mikoláš, M.; Janda, P.; Synek, M.; Marchand, W.; et al. Large old trees increase growth under shifting climatic constraints: Aligning tree longevity and individual growth dynamics in primary mountain spruce forests. *Glob. Change Biol.* **2023**, *29*, 143–164. [CrossRef]
59. Hein, S.; Spiecker, H. 4.3 Controlling Diameter Growth of Common Ash, Sycamore and Wild Cherry. *Valuab. Broadleaved For. Eur.* **2009**, *22*, 123.
60. Hastings, J.H.; Ollinger, S.V.; Ouimette, A.P.; Sanders-DeMott, R.; Palace, M.W.; Ducey, M.J.; Sullivan, F.B.; Basler, D.; Orwig, D.A. Tree Species Traits Determine the Success of LiDAR-Based Crown Mapping in a Mixed Temperate Forest. *Remote Sens.* **2020**, *12*, 309. [CrossRef]